Pergamon

Geochimica et Cosmochimica Acta, Vol. 68, No. 1, pp. 115–125, 2004

0016-7037/04 $30.00 + .00

doi:10.1016/S0016-7037(03)00415-0

Isotopic evidence for trapped fissiogenic REE and nucleogenic Pu in apatite and Pb evolution at the Oklo natural reactor

KENJI HORIE,[1] HIROSHI HIDAKA,*[,1] and FRANÇOIS GAUTHIER-LAFAYE[2]

[1]Department of Earth and Planetary Systems Science, Hiroshima University, Higashi-Hiroshima 739-8526, Japan
[2]Ecole et Observatoire des Sciences de la Terre, UMR7517-CNRS-ULP, 1 rue Blessig, 67084 Strasbourg, France

(*Received December* 30, 2002; *accepted in revised form April* 8, 2003)

Abstract—A part of the boundary layer of reactor zone 10 at the Oklo natural reactor shows a unique petrologic texture, which contains high-grade uraninite and massive apatite concretions. In order to study distribution behavior of fission products around the boundary between the reactor zone and the wall rock and to clarify the relation of migration mechanisms of fission products with geochemical factors, *in-situ* isotopic analyses of Nd, Sm, Gd, Pb and U in uraninite and apatite from the sample were performed by Sensitive High Resolution Ion Microprobe (SHRIMP). Sm and Gd isotopic ratios of uraninite and apatite show evidence of neutron irradiation with fluence between $4.4-6.8\times10^{19}$ n/cm^2. Judging from the isotopic anomalies of Nd and U, the apatite coexisting with the uraninite plays an important role in trapping fissiogenic LREE and nucleogenic ^{239}Pu into the structure. Systematic Pb isotopic data from apatite, uraninite, galena and minium suggest the following chronological interpretations.

1. The apatite formed 1.92 ± 0.01 Ga ago and trapped fissiogenic light REE and nucleogenic ^{239}Pu that migrated from the reactor during the criticality.
2. The uraninite around the boundary between reactor and sandstone dissolved once 1.1∼1.2 Ga ago.
3. Galena grains were formed by U-Pb mobilization in association with the intrusion of dolerite dyke 0.45∼0.83 Ga ago.
4. Minium was derived from recent dissolution of galena under locally oxidizing conditions.

1. INTRODUCTION

Study of elemental transport in association with alteration of uranium minerals is an important consideration in nuclear waste disposal into geological media, because the solubility of uranium changes depending on the redox conditions. It is difficult to address long-term safety issues of a spent fuel repository from just laboratory experiments. Natural analog is generally defined as an occurrence of natural materials relevant to the geological disposal of radioactive waste, which is useful for the investigation of long-termed fixation and/or release processes of radioactive elements controlled by geochemical conditions. Large uranium ore deposits such as Jabiluka, Koongarra, Nabarlek and Ranger at the Alligator River Uranium Fields (Australia) and Cigar Lake (Canada) are useful as natural analogues (Cramer and Smellie, 1992; Maravic and Smellie, 1992). Of particular interest are the naturally occurring fission reactors discovered in the Oklo uranium deposit, Republic of Gabon (I.A.E.A., 1975, 1978). Natural fission reactors are zoned bodies consisting of the reactor core (U content ranging from 20−87 wt.%) enveloped by a clay mantle. Since the discovery of the first reactor zone (hereafter RZ) in 1972 (Bodu et al., 1972; Neuilly et al., 1972), sixteen RZs have been identified at the deposit, and numbered in their chronological order of discovery. Two more RZs were found at Okélobondo adjacent to the Oklo deposit and at Bangombé 30 km south of Oklo. Figure 1 shows a map of the Oklo-Okélobondo uranium deposit and the location of RZs. There is a major difference in magnitude of recent weathering between RZs 1–9 and RZs 10–16, which is due to the oxidizing condition caused by the different burial depths of the RZs from the ground surface. RZ10 is one of the deepest reactors (310 m deep at an altitude of 140 m) and the most preserved from any post-reaction alteration (Gauthier-Lafaye et al., 1996; Hidaka and Holliger, 1998).

Isotopic data from the Oklo RZ samples provide key information to identify the existence of fission products and characterize the nuclear reactions by neutron fluence, reactor temperature, operation duration, etc. Up to now, detailed migration behavior of many kinds of fission products in and around RZs have been reported on the basis of isotopic studies (Loubet and Allegre, 1977; Holliger and Devillers, 1981; Hidaka et al., 1988; Curtis et al., 1989; Loss et al., 1989; Menet et al., 1992; Bros et al., 1993, 1996; Hidaka and Holliger, 1998; Janeczek, 1999; Hidaka and Gauthier-Lafaye, 2000). Most of previous the isotopic studies are based on bulk analysis of the rock samples, and offer geochemical information about fission products at the macro scale ranging from cm to m order. Interest has now shifted towards obtaining the distribution behavior of fission products in individual minerals which are included in the rock samples. In situ isotopic observation with secondary ion mass spectrometry (SIMS) has been widely used in the field of geology and geochemistry, and make it possible to investigate the distribution behavior of the elements in micro region ranging from a few μm to a few tens μm. Previous results from SIMS analysis of Oklo samples suggest a significant role of selective fixation of migrating fission products into specific

* Author to whom correspondence should be addressed (hidaka@hiroshima-u.ac.jp).

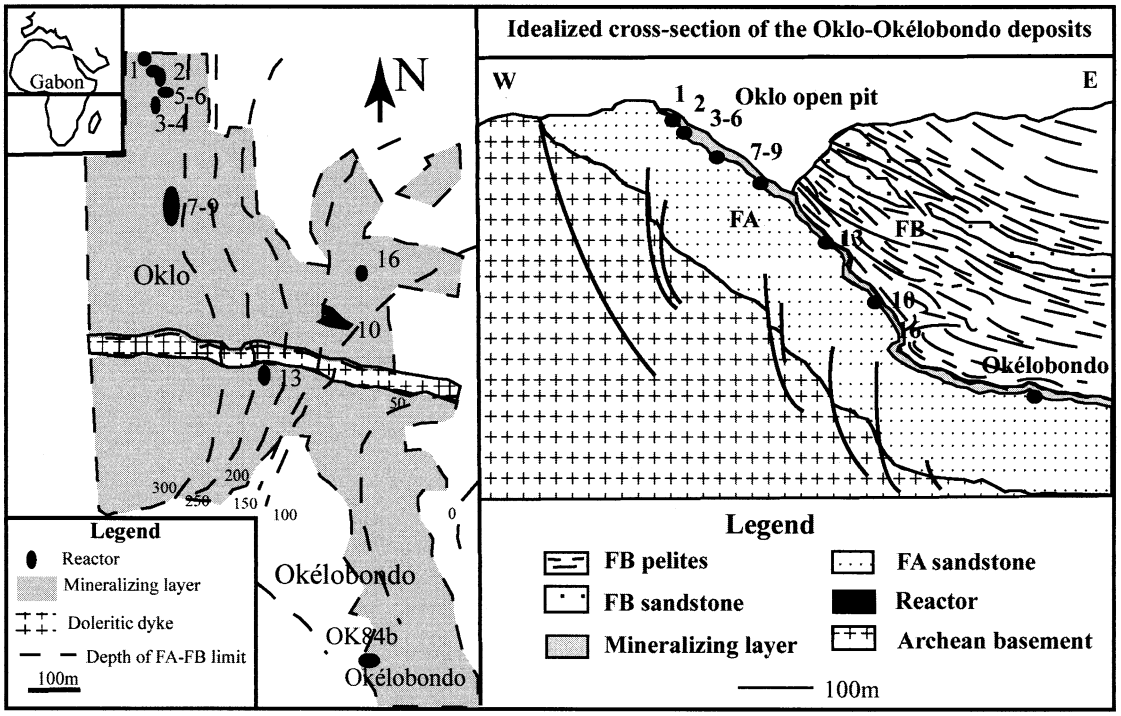

Fig. 1. Map of the Oklo-Okélobondo uranium deposit. Sketch in the left shows location of the reactor zones. The right figure shows cross section of the deposit with the depth location of the reactor zones (modified after Gauthier-Lafaye et al., 1996).

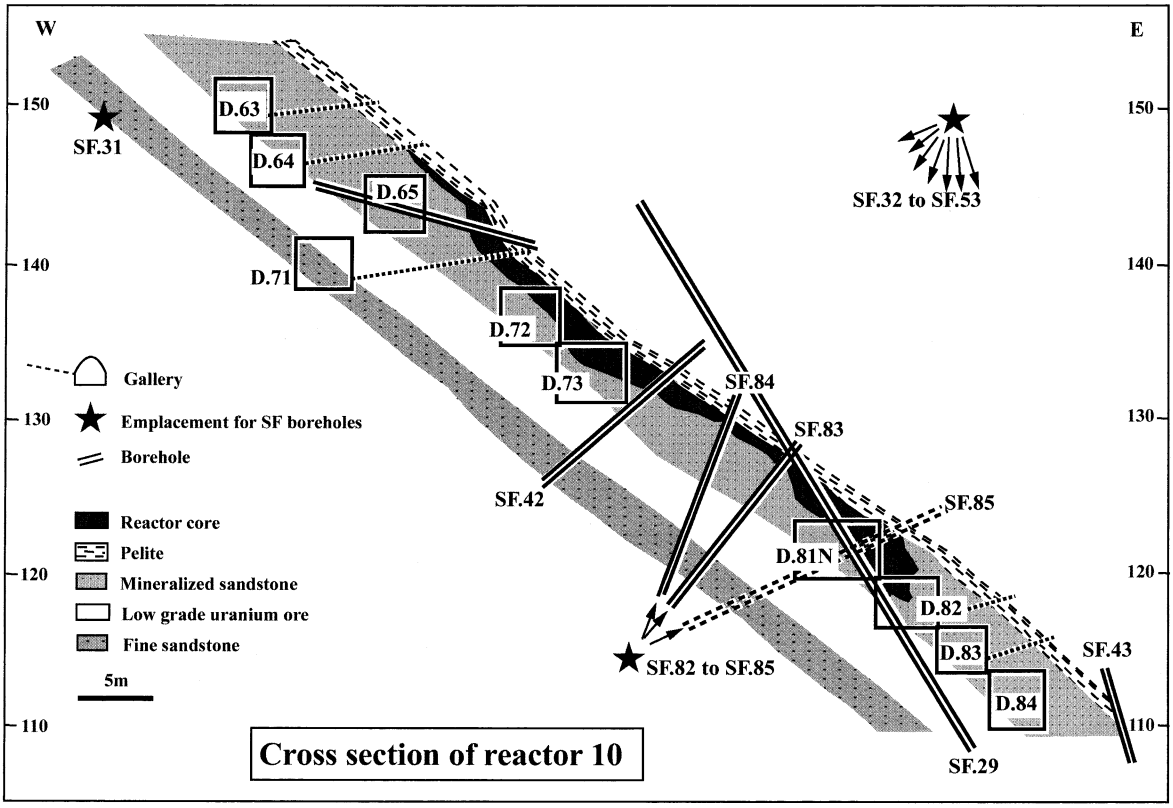

Fig. 2. Cross section of RZ10

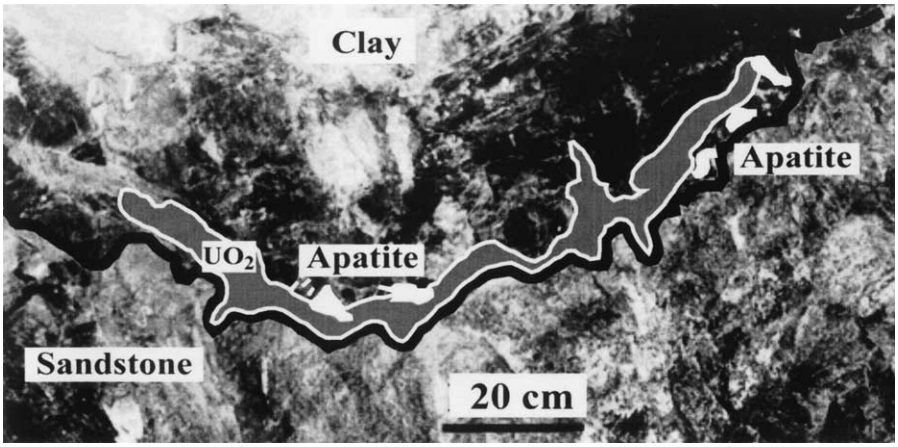

Fig. 3. Outline of the boundary between RZ10 and sandstone layer around D81. Enrichement of uraninite and apatite concretions can be seen between clay and sandstone layers. Scale bar is 20 cm.

minerals: REE in florencite (Janeczek and Ewing, 1996; Dymkov et al., 1997) and platinum group elements in metallic aggregates (Gauthier-Lafaye et al., 1996; Hidaka et al., 1999). In this paper, we report the distribution behavior of fissiogenic REE in uraninite and apatite, and the possibility of fixation of Pu into apatite from isotopic results via Sensitive High Resolution Ion Microprobe (SHRIMP). Pb isotopic compositions of uraninite, apatite and Pb minerals were also analyzed to provide a chronological discussion of the alteration history of the uraninite.

2. MATERIAL AND METHODS

2.1. Samples

2.1.1. Oklo sample

RZ10 is the most studied among the recently discovered RZs 10–16 (Menet et al., 1992; Bros et al., 1993; Hidaka et al., 1993; Hidaka and Holliger, 1998). The cross section of RZ10 is shown in Figure 2. The RZ10 is about 50 cm thickness, 30 m wide, and 27 m long. Thirteen boreholes and five drifts provide access to the RZ. D81 is one of the drifts faced to the RZ. Sample D81–13 used in this study was taken from a boundary between RZ10 and a sandstone layer just beneath the reactor. The boundary shows a unique petrologic texture, which contains high-grade uraninite and massive apatite concretions (Fig. 3). Figure 4 shows a SEM photomicrograph of a thin section sample D81–13. The petrologic texture of D81–13 suggests that the sample was subjected to the interaction with fluid that flowed after cessation of nuclear reactions. The sample mainly consists of uraninite and apatite, and includes some clay minerals (illite and chlorite). As minor components, Pb minerals such as galena (PbS) and minium (Pb_3O_4) are found in the sample. More than one hundred of galena grains, ranging from 20–30 μm in size, are scattered throughout the uraninite matrix. Only two minium grains about 10 and 30 μm in size were found in fine fractures within an apatite grain. Minium is a rare mineral which is considered to be formed under strong oxidizing environment (Savaray and Pagel, 1997).

2.1.2. Standard uraninite and apatite

The Faraday Mine uraninite and PRAP apatite were used as standard materials for REE measurements of uraninite and apatite, respectively. The Faraday Mine uraninite deposit occurs in a belt of metagabbro and amphibolite on the south flank of the Faraday granite at Bancroft, Ontario, Canada. The ore bodies are parts of a system of pegmatitic granite dykes found at intervals of over 6000 feet and a width of several hundred feet (Leng et al., 1962). The sample used in this study is a fragment of a massive uraninite grain. PRAP apatite was from the Prairie Lake carbonatite complex, Ontario, Canada (Sano et al., 1999).

2.2. Analytical Procedures

In situ isotopic analyses of Pb, U and REE were performed on a SHRIMP II at Hiroshima University. The sample was mounted with standard minerals in an epoxy resin disk, and polished with 1/4 μm diamond paste. A 2.2–2.5 nA beam of O_2^- primary ion was used to scatter a 20 μm analytical spot on the sample. Before SHRIMP measurements, analytical spots were selected by using a BSE image to avoid micro fractures and inclusions. The $^{204}Pb^+$, $^{206}Pb^+$, $^{207}Pb^+$, $^{208}Pb^+$, $^{235}U^+$ and $^{238}U^+$ peaks were measured with a mass resolution of about 5800 (M/ΔM at 1% of peak height) for Pb and U isotopic analysis. For REE analysis of uraninite, masses from $^{139}La^+$ to $^{175}Lu^+$ and $^{238}U^+$ were scanned. In the case of apatite, masses from $^{139}La^+$ to $^{175}Lu^+$ were scanned together with $^{159}(Ca_2PO_3)^+$ as a derivative ion species from major elements of apatite. To avoid isobaric interferences from light REE oxide species onto heavy REE mono-atomic species, high mass resolution condition (M/ΔM=9200) was used.

For the determination of the REE elemental abundances of the samples, a simple calibration method, via the comparison of secondary ion ratios between standard materials and analytical sample, is often used for quantitative SIMS analysis. To calibrate secondary ion count rates of REE to the absolute elemental abundances, determination of sensitivity factors for individual REE is required in SHRIMP analysis. The Faraday uraninite was crushed, and then five of the fragments were separately powdered. One to two mg of each fraction was gently dissolved with 2 mol/L HNO_3. The dissolved fractions were individually diluted to 15 mL with 0.5 mol/L HNO_3, and the REE contents of each solution were measured by ICP-MS (Micromass PQ III) to confirm the homogeneity of REE contents between fragments. The same treatments were performed on the PRAP apatite. From the analytical data of the Faraday Mine uraninite, the conversion factor (f_i) of secondary ion intensity of each REE (REE_i^+) to the concentration, [REE_i], is given by the following equations.

$$f_i = \frac{[REE_i]}{REE_i^+/^{238}U^+} \text{ for uraninite, and}$$

$$f_i = \frac{[REE_i]}{REE_i^+/^{159}(Ca_2PO_3)^+} \text{ for apatite.}$$

Then, REE concentrations of unknown sample can be determined from SHRIMP analytical data by use of the f_i. The f_i values for uraninite and apatite are summarized in Table 1. This method cannot be simply

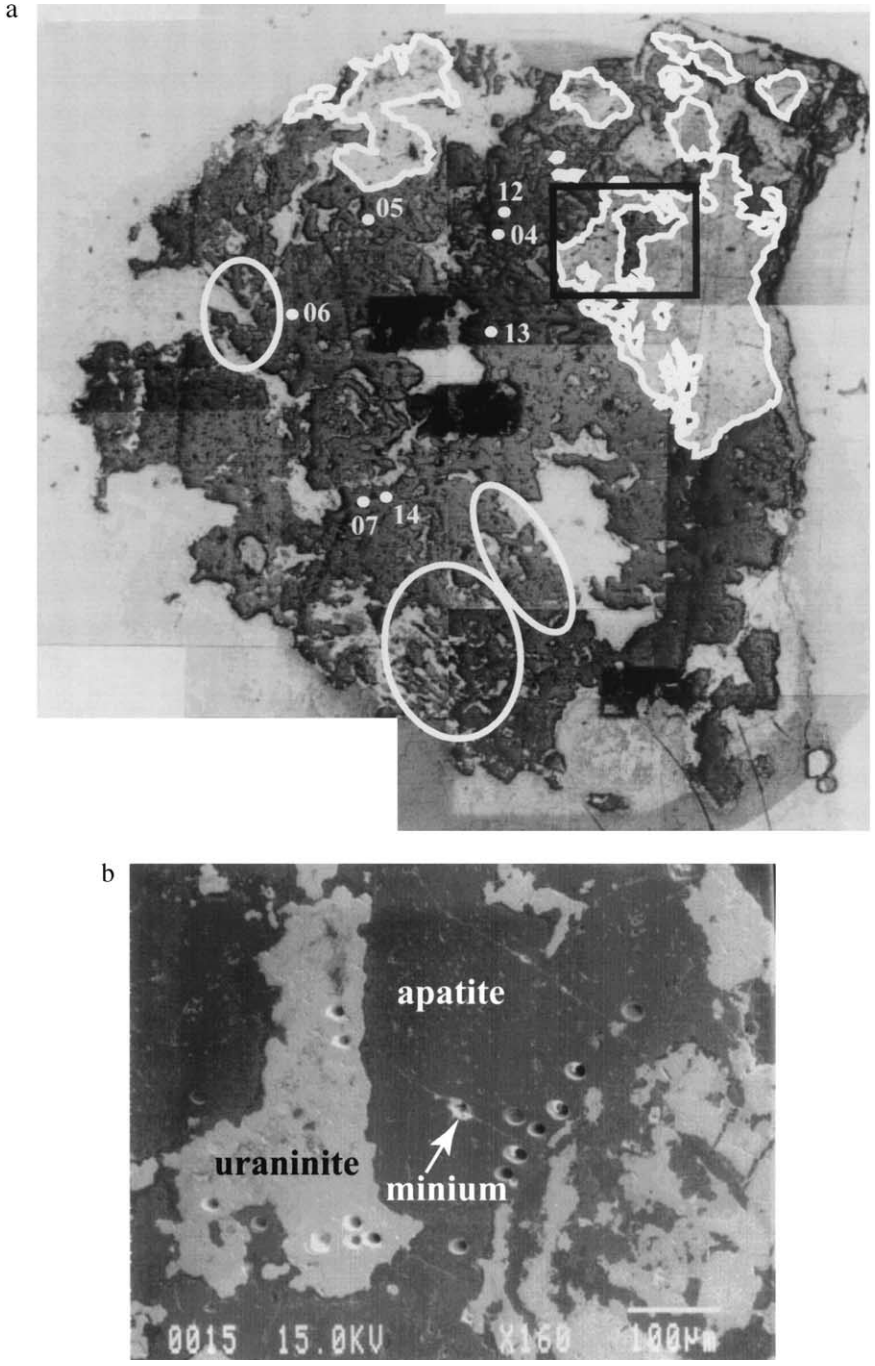

Fig. 4. (a) Optical micrograph of thin section sample D81-13 taken from the boundary between RZ10 and sandstone layer. The number in the photo corresponds to the analytical spot of uraninite described in Table 3. Petrologic texture in the circled region suggest the dissolution of uraninite. Bold region in black is enlarged to (b). (b) Back scattered electron image of thin section of D81-13. Craters in the photo are analytical spots for SHRIMP measurement. Scale bar is 100 mm.

applied for the analysis of the Oklo samples, because most elements in the Oklo samples have isotopic anomalies due to nuclear reactions. In general, the LREE (La, Ce, Nd, Sm) of RZ samples show larger isotopic anomalies than the HREE (Dy, Er, Yb, Lu) because of the difference of product yields from ^{235}U-fission. Before quantitative analysis, all isotopic abundances of each REE in a sample have to be known. However, it is impossible to perform full isotopic analyses for individual elements by in situ measurements, because of the presence of complex isobaric interferences on the mass spectrum. On the basis of the previous isotopic studies, it can be considered that the REE isotopic compositions of any reactor core samples are roughly homogeneous in RZ10 except for a few isotopes such as ^{152}Gd (Hidaka and Holliger, 1998; Hidaka and Gauthier-Lafaye, 2000). Assuming that elements in the sample located around the boundary of the RZ have been formed from mixtures of two components, reactor materials (fissiogenic component) and host-rock (non-fissiogenic component), the isotopic abundances of any element, which could not be directly obtained by in situ measurements, were calculated as two-component

Table 1. Conversion factors (f_i) of uraninite and apatite.

	uraninite	apatite
La	6.51×10^3	8.06×10^3
Ce	3.98×10^3	1.28×10^4
Pr	2.52×10^3	1.03×10^4
Nd	2.16×10^3	8.41×10^3
Sm	1.12×10^3	8.72×10^3
Eu	9.04×10^2	6.92×10^3
Gd	2.31×10^4	5.54×10^4
Tb	9.49×10^3	2.78×10^4
Dy	1.65×10^4	1.10×10^5
Ho	5.40×10^3	2.55×10^4
Er	2.09×10^4	1.04×10^5
Tm	4.47×10^3	4.28×10^4
Yb	1.05×10^4	1.57×10^5
Lu	3.24×10^4	1.09×10^5

mixtures having different isotopic compositions. The mixing proportion of the two components was understood from isotopic abundances of direct measurements.

To find minium in the thin section sample, micro-Raman analyses were performed using SEM-Raman (JEOL JRS-SYSTEM 3000) at Ehime University. Analytical spot by Ar laser was 2 μm. Minium was identified from three characteristic peaks around 83, 136, and 269 cm^{-1} on the Raman spectrum (Savary and Pagel, 1997).

3. RESULTS AND DISCUSSION

Many elements of the Oklo samples have isotopic anomalies caused mainly by fission and neutron capture reactions. It is convenient to use isotopic ratios of REE to define characteristics of the Oklo reactors, because of high fission yields of LREE and high sensitivities of Sm and Gd isotopes for neutron flux. In addition, combination of U and REE isotopic data can be used to determine nuclear parameters of natural reactors (e.g., Gauthier-Lafaye et al., 1996; Hidaka and Holliger, 1998). In the case of in situ isotopic analyses, only isotopes with small isobaric interferences are available for further discussion. Therefore, the isotopic ratios $^{143}Nd/^{146}Nd$, $^{149}Sm/^{147}Sm$, $^{155}Gd/^{160}Gd$, $^{156}Gd/^{160}Gd$, $^{157}Gd/^{160}Gd$, $^{158}Gd/^{160}Gd$ and $^{235}U/^{238}U$ have been used to characterize the samples in this study. Isotopic data of uraninite and apatite are compiled in Tables 1 and 2.

3.1. Isotopic ratios of Nd, Sm, Gd and U in Uraninite and Apatite

3.1.1. Nd isotopic ratios ($^{143}Nd/^{146}Nd$)

$^{143}Nd/^{146}Nd$ isotopic ratios are variable even in common silicate rocks, because the long-lived radioisotope ^{147}Sm ($t_{1/2}$ = 106 Ga) decays to ^{143}Nd. In general, isotopic variation of the $^{143}Nd/^{146}Nd$ ratio due to fission reactions is much larger than that of decay from ^{147}Sm. High $^{143}Nd/^{146}Nd$ ratio provides evidence for the contribution of fissiogenic Nd ($^{143}Nd/^{146}Nd$=1.95, see Table 2) into samples, because the fission yields of Nd isotopes exponentially decrease with their mass numbers (e.g., Hidaka et al., 1988). Nd isotopic ratios of apatite and uraninite in D81-13 sample indicate large contribution of fissiogenic components. As shown in Table 2, the small variations of $^{143}Nd/^{146}Nd$ ratios of PRAP (0.707±0.003) and the Faraday Mine uraninite (0.724±0.020) are attributed to the α-decay of ^{147}Sm, and the values depend upon the elemental abundance of Sm/Nd in individual samples. On the other hand, the uraninite and apatite of sample D81-13 show much larger $^{143}Nd/^{146}Nd$ ratios (1.904±0.036 for uraninite and

Table 2. Isotopic ratios of Nd, Sm and Gd in apatite and uraninite.

	$^{143}Nd/^{146}Nd$	$^{149}Sm/^{147}Sm$		
fissiogenic* (calculated)	1.95			
PRAP	0.707 ± 3	0.917 ± 9		
FM uraninite	0.724 ± 20	0.922 ± 19		
D81-13 apatite	1.843 ± 20	0.00314 ± 50		
D81-13 uraninite	1.904 ± 36	0.0162 ± 2		
RZ10 core**	1.619–1.736	0.0053–0.0100		
	$^{155}Gd/^{160}Gd$	$^{156}Gd/^{160}Gd$	$^{157}Gd/^{160}Gd$	$^{158}Gd/^{160}Gd$
PRAP	0.668 ± 25	0.964 ± 54	0.714 ± 19	1.121 ± 19
FM uraninite	0.698 ± 13	0.966 ± 38	0.710 ± 7	1.114 ± 25
D81-13 apatite	0.139 ± 10	1.556 ± 37	0.0776 ± 131	1.735 ± 85
D81-13 uraninite	0.240 ± 17	2.547 ± 124	0.1492 ± 73	2.258 ± 156
RZ10 core**	0.0356–0.0469	2.381–2.731	0.00373–0.0216	2.048–2.163
	$^{(155+156)}Gd/^{160}Gd$	$^{(157+158)}Gd/^{160}Gd$		
fissiogenic* (calculated)	77.24	19.06		
PRAP	1.662 ± 60	1.834 ± 28		
FM uraninite	1.664 ± 40	1.820 ± 31		
D81-13 apatite	1.699 ± 41	1.820 ± 91		
D81-13 uraninite	2.790 ± 20	2.409 ± 160		
RZ10 core**	2.428–2.766	2.066–2.167		

All standard errors indicated the last digit are 1σ of the mean.

* Isotopic ratios of fissiogenic component are calculated from the fission yields by England and Rider (1993) on the assumption of fission inventory as ^{235}U (92%) + ^{238}U (4%) + ^{239}Pu (4%).

** Data from Hidaka and Holliger (1998).

1.843±0.020 for apatite) than the standard minerals. It is considered that the isotopic ratios of the sample resulted from mixing of fissiogenic and non-fissiogenic components, and in this case, the uraninite and apatite grains contain a large amount of fissiogenic Nd relative to non-fissiogenic Nd. Previous study on determination of nuclear parameters of RZ10 shows that the fission inventory of RZ10 is 90–92% for ^{235}U fission and 2–5% for ^{238}U and ^{239}Pu fission (Hidaka and Holliger, 1998). Calculated value for fissiogenic ^{143}Nd/^{146}Nd ratio of RZ10 is 1.95 on the assumption of typical inventory, 92% for ^{235}U fission and 4% for ^{238}U and ^{239}Pu fission. For the calculation, the data of fission yields were cited from England and Rider (1993). Considering the simple mixing model by two components, fissiogenic (^{143}Nd/^{146}Nd=1.95) and non-fissiogenic origin (^{143}Nd/^{146}Nd=0.70 and 0.72 for apatite and uraninite, respectively), the contribution of fissiogenic Nd component in the total amount of Nd is calculated at 96±4% for uraninite and 91±2% for apatite.

3.1.2. Sm and Gd isotopic ratios

Only ^{149}Sm and ^{147}Sm of seven Sm stable isotopes are free of isobaric interferences and can be reliably measured by SHRIMP analysis. Since ^{149}Sm has a very large neutron capture cross section (σ=4.2×10^4 barn for thermal neutron), its isotopic abundance is extremely depleted under the intensive neutron fluence in RZ. Therefore ^{149}Sm isotopic deficit can be used to quantify the neutron fluence. As shown in Table 2, ^{149}Sm/^{147}Sm values of RZ sample show remarkable depletion relative to those of PRAP and the Faraday uraninite.

Significant isotopic evidence for neutron capture reactions can also be seen in the Gd isotopic ratios. Isotopic depletions of ^{155}Gd and ^{157}Gd, and isotopic enrichments of ^{156}Gd and ^{158}Gd indicate the occurrence of the neutron capture reactions ^{155}Gd(n,γ)^{156}Gd and ^{157}Gd(n,γ)^{158}Gd. Neutron capture reactions provide isotopic depletion of ^{155}Gd and ^{157}Gd quantitatively corresponding to isotopic enrichment of ^{156}Gd and ^{158}Gd, respectively. In the case of Gd isotopic measurements by SHRIMP analysis, only ^{155}Gd and ^{157}Gd are free of isobaric interferences. Although ^{156}Gd, ^{158}Gd and ^{160}Gd have isobaric interferences from Dy, there are few isobaric interferences of Dy isotopes on the Gd mass spectra because of lower elemental abundance of Dy relative to Gd (Dy/Gd=0.36~0.64 for RZ10; Hidaka and Holliger, 1998) and the small isotopic abundances of ^{156}Dy, ^{158}Dy and ^{160}Dy. Judging from previous isotopic studies of Oklo samples, the isotopic compositions of Dy in the Oklo reactor samples are generally considered to be little different from non-fissiogenic compositions because of low fission yields and small neutron capture cross sections of Dy isotopes (Hidaka et al., 1988). The isotopic abundances of ^{156}Gd, ^{158}Gd and ^{160}Gd were corrected by monitoring of ^{163}Dy abundance on the assumption of no disturbance to the ^{156}Dy, ^{158}Dy, ^{160}Dy and ^{163}Dy isotopic abundances by fission reactions.

The Gd isotopic ratios of uraninite and apatite are shown in Table 2. ^{160}Gd is only little influenced by nuclear reactions, because of shielding from β^- decay and a very small neutron capture cross section (60 barn). Isotopic depletion of ^{155}Gd/^{160}Gd and ^{157}Gd/^{160}Gd and enrichment of ^{156}Gd/^{160}Gd and ^{158}Gd/^{160}Gd in the uraninite and apatite show strong evidence of neutron capture reactions. The effects of ^{156}Gd(n,γ)^{157}Gd and ^{158}Gd(n,γ)^{159}Gd are negligible, because the neutron capture cross sections of ^{156}Gd (2 barn) and ^{158}Gd (2.4 barn) are very small. Therefore, (^{155}Gd + ^{156}Gd)/^{160}Gd and (^{157}Gd + ^{158}Gd)/^{160}Gd ratios should be constant if they were only disturbed by neutron capture reactions. As shown in literature data of Table 2, Gd isotopic compositions of Oklo samples are generally influenced not only by neutron capture reactions but also by contamination of fission products. In general, the samples taken from the core of RZ10 contain 1–1.4% fissiogenic Gd (Hidaka and Holliger, 1998). The content of fissiogenic Gd in D81-13 uraninite is nearly equal to those of reactor core samples. On the other hand, D81-13 apatite shows less than 0.05% of fissiogenic Gd. From the calibration of the ^{157}Gd-^{158}Gd isotopic shifts of experimentally neutron-irradiated Gd redundant reagent (Hidaka et al., 1995), neutron fluence (Ψ neutrons/cm^2) of the sample can be calculated as follows.

$$\psi = \frac{(^{158}Gd/^{157}Gd)_{sample} - (^{158}Gd/^{157}Gd)_{STD0}}{(^{158}Gd/^{157}Gd)_{STD1} - (^{158}Gd/^{157}Gd)_{STD0}} \times (1.4 \times 10^{16})$$

where (^{158}Gd/^{157}Gd)$_{STD0}$=1.586784±0.000017 and (^{158}Gd/^{157}Gd)$_{STD1}$=1.591089±0.000010 are the isotopic ratios of the standard materials without neutron irradiation and with artificial neutron irradiation of 1.4×10^{16} neutrons/cm^2, respectively (Hidaka et al., 1995). The calculation provides neutron fluences of (4.4±0.4)×10^{19} and (6.8±1.3)×10^{19} n/cm^2 for D81-13 uraninite and apatite, respectively. Considering the neutron fluence values for RZ10 SF-84 core series samples, the values for D81-13 at the boundary of RZ10 may be reasonable. These values are more than 10 times lower than the neutron fluences for RZ10 SF-84 core samples, 5.3–8.0×10^{20} n/cm^2 (Hidaka and Holliger, 1998). In addition, the host-rock sandstone (SF84-1400) taken from a 60cm below the RZ10 shows a neutron fluence of 6.2×10^{18} n/cm^2 (Hidaka and Holliger, 1998). Significant difference can be seen in the neutron fluence values between the uraninite and apatite. However, there is a possibility of underestimation for the neutron fluence of the uraninite, because the uraninite includes a small amount of fissiogenic Gd isotopes. On the other hand, the neutron fluence of the apatite reflects the neutron fluence value at the boundary between RZ and sandstone, because the Gd isotopic composition of apatite is little subject to fission products.

3.1.3. U isotopic ratios (^{235}U/^{238}U)

D81-13 uraninite shows evidence of ^{235}U fission, because the ^{235}U isotopic abundance is depleted. The ^{235}U/^{238}U isotopic ratios from eight different analytical spots in individual grains are constant within analytical errors, which indicate U isotopic homogeneity in the uraninite grain. However, the ^{235}U/^{238}U values ranging 0.00659–0.00666 are slightly higher than those of SF84 core samples (^{235}U/^{238}U=0.00507–0.00605). Considering the neutron fluence of D81-13 uraninite is much lower than those of SF84 core, the degree of depletion of ^{235}U/^{238}U in the D81-13 uraninite may be reasonable. The existence of only two tiny minium grains in an apatite grain coexisting with the uraninite and textual evidence of hydrothermal circulation in the uraninite (Fig. 4(a)) suggest that the uraninite once dissolved under locally oxidizing condition. If

Table 3. Isotopic ratios of Pb and U in apatite and uraninite and U concentration in apatite.

(a) Pb and U

	$^{204}Pb/^{206}Pb$	$^{207}Pb/^{206}Pb$	$^{208}Pb/^{206}Pb$	$^{235}U/^{238}U$	age (Ma)
Faraday Mine uraninite					
01				0.00730 ± 1	
02				0.00729 ± 2	
03				0.00725 ± 3	
04				0.00729 ± 2	
05				0.00728 ± 2	
uraninite					
01	0.0000541 ± 14	0.0753 ± 4	0.00290 ± 7	0.00663 ± 2	1254 ± 11
02	0.0000459 ± 10	0.0721 ± 2	0.00225 ± 2	0.00664 ± 2	1166 ± 8
03	0.0000644 ± 27	0.0765 ± 4	0.00308 ± 8	0.00659 ± 2	1297 ± 12
04	0.0000346 ± 11	0.0694 ± 2	0.00196 ± 2	0.00666 ± 2	1084 ± 8
05	0.0000486 ± 21	0.0726 ± 4	0.00277 ± 5	0.00661 ± 2	1189 ± 12
06	0.0000396 ± 41	0.0700 ± 2	0.00214 ± 4	0.00659 ± 3	1123 ± 10
07	0.0000405 ± 29	0.0702 ± 2	0.00202 ± 4	0.00663 ± 2	1116 ± 8
08	0.0000651 ± 37	0.0804 ± 4	0.00393 ± 4	0.00661 ± 8	1387 ± 25
09	0.0000445 ± 5	0.0715 ± 1	0.00229 ± 1		1162 ± 2
10	0.0000884 ± 7	0.0850 ± 2	0.00448 ± 4		1497 ± 4
11	0.0000602 ± 8	0.0735 ± 4	0.00280 ± 4		1216 ± 10
12	0.0000524 ± 9	0.0724 ± 6	0.00251 ± 3		1186 ± 16
13	0.0000470 ± 6	0.0710 ± 5	0.00235 ± 3		1148 ± 13
14	0.0000616 ± 12	0.0743 ± 5	0.00314 ± 3		1237 ± 13
PRAP					
01				0.00769 ± 26	
02				0.00727 ± 6	
03				0.00772 ± 21	
04				0.00756 ± 21	
apatite					
01	0.000212 ± 5	0.1323 ± 5	0.00833 ± 4		
02	0.000244 ± 9	0.1172 ± 5	0.00989 ± 16	0.00730 ± 11	
03	0.000324 ± 21	0.1333 ± 22	0.0122 ± 37	0.01303 ± 102	
04	0.000241 ± 11	0.1287 ± 8	0.00942 ± 11		
05	0.000244 ± 8	0.1260 ± 8	0.00828 ± 6		
09				0.00944 ± 83	
10				0.01707 ± 57	
11				0.01346 ± 44	

(b) U concentration of apatite (ppm)

07	67.6 ± 3.5
08	553 ± 134
09	57.3 ± 0.9
10	72.8 ± 4.8

The age of uraninite 09–14 were calculated by using $^{235}U/^{238}U = 0.0066$.
All standard errors indicated the last digit are 1σ of the mean.
The analytical number of uraninite and apatite is consistent between tables (a) and (b).

so, there is a possibility that ^{235}U-depleted uranium mixed with normal uranium around the boundary region by dissolution and then co-precipitated. Simple calculation on the assumption of mixing of two components, resulted in 60–75% of normal uranium ($^{235}U/^{238}U=0.00725$) and 25–40% of ^{235}U-depleted uranium as an apparent mixing proportion for the D81-13 uraninite. However, if such a large amount of normal uranium mixed with ^{235}U-depleted uranium through dissolution process, existence of fissiogenic Nd or Sm would not be sufficiently obvious in the isotopic compositions. Therefore, judging from the isotopic systematics of REE and U, the possibility of contamination of normal uraninite into D81-13 uraninite seems very low even if the dissolution of uraninite occurred. It has been concluded that the isotopic data from D81-13 uraninite reflect the fission event around the boundary layers.

Although U isotopic data of apatite include large analytical errors because of low U content (57–550 ppm), significant ^{235}U excesses ($^{235}U/^{238}U>0.013$), greater than analytical error (see Table 3(a)), are observed from at least five analytical spots in the apatite. Isotopic excess of ^{235}U in Oklo samples is extremely rare, but a few examples have been observed in clay minerals and apatite (Bros et al., 1993; 1996). ^{235}U excess is interpreted as a result of selective uptake of ^{239}Pu in association with chemical fractionation between U and Pu. In this case, it may be reasonable that Pu was trapped into the apatite grain. LREE and especially Nd are often used as geochemical analogues of Pu (Lugmair and Marti, 1977; Chapman and Smellie, 1986). Pu might be present as trivalent form under reducing conditions, and behaved with other trivalent species such as Nd. The enrichment of fissiogenic Nd in the apatite also suggests the selective uptake of Pu in the apatite.

3.1.4. Origin of isotopic anomalies in apatite

The apatite beneath RZ10 may play an important role in incorporating fissiogenic REE and Pu. It is worth noting that there is a significant difference in the isotopic variations of Nd, Sm and Gd between apatite and uraninite. Systematic interpretations of REE and U isotopic data provide information on migration behavior of fissiogenic REE and actinide elements because of the similarity of chemical properties between REE and U (Hidaka and Holliger, 1998; Hidaka and Gauthier-Lafaye, 2000). There are two interpretations to explain the origin of isotopic anomalies from the isotopic results of D81-13 samples used in this study: (1) trapping of fissiogenic components from the reactor core; (2) in situ fission in the minerals. As mentioned above, isotopic anomalies in the uraninite are derived from in situ fission. The origin of fissiogenic isotopes in the apatite is considered to be different from that of uraninite. Uranium content in the apatite, 57–550 ppm, is too low to accumulate significant amount of fissiogenic components by in situ fission in the grain. Gd in the apatite is the best example to understand where the isotopic anomalies occurred. Little addition of fissiogenic component and strong evidence of neutron capture effects on the Gd isotopes, shown in Table 2, suggest that the isotopic anomalies of Gd are simply derived from interaction of neutrons coming from the reactor into the apatite. On the other hand, more than 90% of the Nd in the apatite is fissiogenic. It is reasonable to interpret that a large amount of fissiogenic Nd was mobilized during the dissolution of uraninite and trapped into the apatite. Previous study on the REE isotopes of apatite suggests the selective uptake of fissiogenic LREE into apatite grain of the Oklo samples (Hidaka et al., 1994; Raimbault et al., 1996). In this study, it is reasonably concluded that fissiogenic Nd and Sm were preferably incorporated into the apatite grain rather than Gd.

Here, the most important matter is when the apatite formed. Most parts of the apatite with non-depleted ^{235}U ($^{235}U/^{238}U=0.00725$) show a mineralization age of 1.92 ± 0.01 Ga which is close to the occurrence age of criticality. It is generally considered that the Oklo deposit went critical at 1.95 ± 0.03 Ga (Naudet, 1991). The apatite formation should be considered to be equal to the occurrence of reactor criticality, because there is no significant difference between two ages within analytical errors. The D81-13 apatite formed at the same time as the criticality of the reactor, and then incorporated Pu and fissiogenic LREE during the criticality.

3.2. Distribution of REE in Apatite and Uraninite

In general, the elements of the Oklo samples are mixture of fissiogenic and non-fissiogenic components. The REE of the Oklo samples particularly have isotopic anomalies depending on the scale of nuclear reactions, because most REE isotopes have large neutron capture cross sections and high fission yields. It is important to distinguish the inventory of REE contents between fissiogenic and non-fissiogenic fractions to investigate geological and nucleochemical conditions around the natural reactors (Hidaka and Gauthier-Lafaye, 2000).

Figures 5 (a) and 5(b) show REE patterns of D81-13 uraninites and apatites, respectively, normalized to Post-Archean Average Australian Shale (PAAS). Enrichment of LREE (in particular the Pr-Nd-Sm region), decrease from MREE to HREE and zigzags in the HREE region are striking features commonly observed in Oklo RZ samples (Hidaka et al., 1992; Hidaka and Gauthier-Lafaye, 2000). Enrichment of LREE is clearly subjected to accumulation of fissiogenic components. Since the fission product yield exponentially decreases with the mass number, both REE patterns reflect contribution of fissiogenic component.

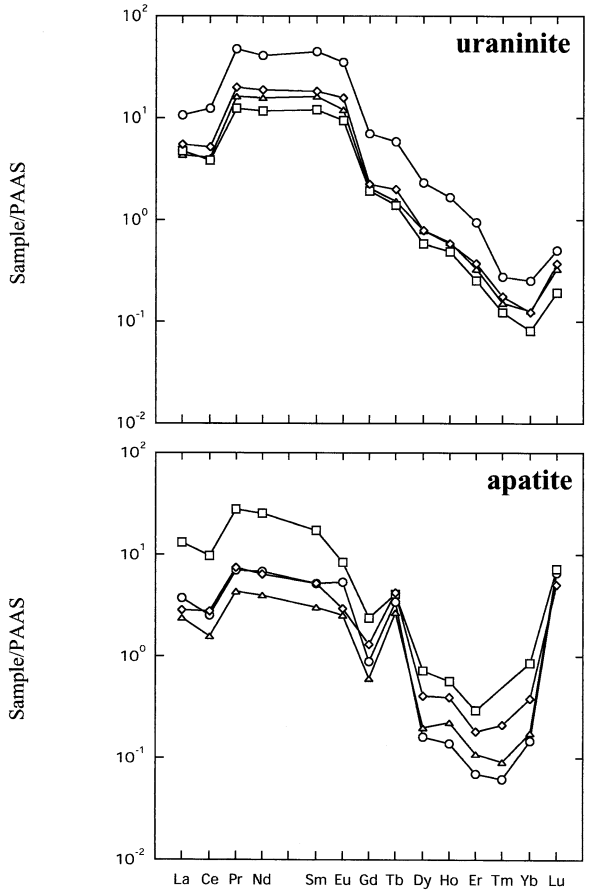

Fig. 5. REE patterns of (a) uraninite and (b) apatite in D81-13. The data are normalized to PAAS.

The REE patterns of uraninite have a clear kink in Er-Tm-Yb-Lu. Judging from small amount of geological alteration of RZ10 (Hidaka and Gauthier-Lafaye, 2000) and low fission yields of HREE, elemental abundances of the HREE reflect a geochemical property of the primary ore. The curve at HREE is considered to be derived from lanthanide tetrad effect, which shows evidence of strong water-rock interaction (Masuda and Ikeuchi, 1979). HREE of the uraninite were distributed in association with the primary ore formation, and were not affected by later alteration. Alteration degree of the Oklo uraninite has been classified by the correlation diagram between total contents of non-fissiogenic REE (ΣREE) vs. REE chemical fractionation (LREE/HREE) (Hidaka and Gauthier-Lafaye, 2000). The data of uraninite measured in this study are plotted in Figure 6 shown the relationship between ΣREE and LREE/HREE. It is reported that the Oklo uraninites with little alteration, such as SF84 samples from RZ10, typically show much

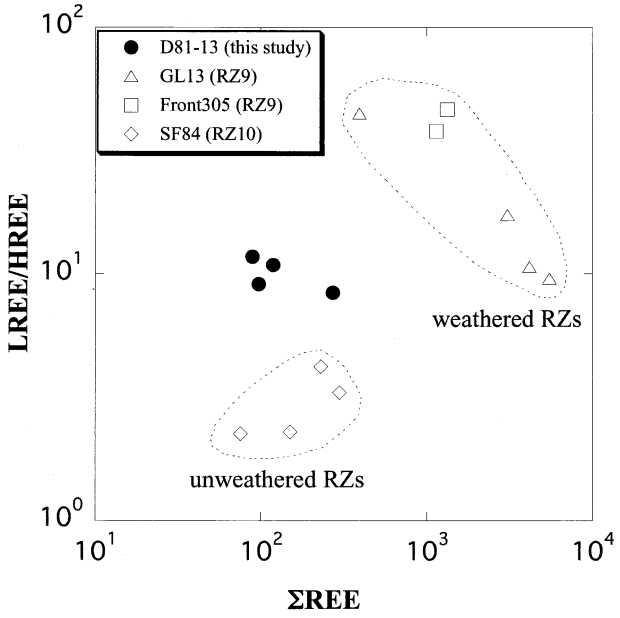

Fig. 6. Plot of total amount of REE (SREE) vs. REE fractionation (LREE/HREE) for RZs samples. The data for GL13, Front 305 and SF84 are cited from Hidaka and Gauthier-Lafaye (2000).

lower ΣREE (<300 ppm) than the altered uraninites. As a result of the calculation of non-fissiogenic REE components of D81-13 uraninite, ΣREE ranges from 89 to 271 ppm. As shown in Figure 6, the data of D81-13 uraninite are differently plotted from the other two groups. The data suggest that the uraninite once dissolved around the boundary between the reactor core and host-rock, but did not incorporate significant amounts of non-fissiogenic REE from the host-rock.

It is considered that the apatite of D81-13 plays an important role in trapping the fissiogenic REE in association with the dissolution of uraninite. Since the Gd isotopic composition of the apatite suffers from neutron capture effects, the apatites were originally located at the reactor boundary and irradiated by neutrons leaked from the reactor. It is well know that apatite selectively includes LREE to MREE in normal geological conditions (McArthur and Walsh, 1984; Felitsyn and Morad, 2002). Considering the REE patterns and isotopic signature of apatites, the apatites selectively took fissiogenic LREE, especially Nd and Sm released from the uraninite in association with dissolution of uraninite.

3.3. Alteration History Inferred from Pb Isotopic Signature

In this study $^{207}Pb/^{206}Pb$ ratios from uraninite and apatite may not necessarily provide direct information of formation ages, because of late dissolution of uraninite and isotopic disturbance from anomalous $^{235}U/^{238}U$ ratios due to fission. However, systematic interpretation of the Pb isotopic signature of the uraninite, apatite and Pb minerals in the sample puts some chronological constraints on the alteration history. Since the isotopic abundance of ^{204}Pb in all uraninite and apatite grains show negligibly low value ($^{204}Pb/^{206}Pb<0.00009$ for uraninite and <0.0004 for apatite) shown in Table 3, the $^{207}Pb/^{206}Pb$ ratios can be used to determine the formation ages of individual minerals without correction of common Pb.

3.3.1. Uraninite and apatite

The D81-13 uraninite has homogeneous U isotopic ratios with a depletion of ^{235}U ($^{235}U/^{238}U=0.0066$), but its Pb isotopic ratios show a slight variation ($^{207}Pb/^{206}Pb=0.0694\sim0.0804$). This suggests that chemical fractionation between U and Pb occurred in association with dissolution of uraninite. The $^{207}Pb/^{206}Pb$ ratios of the uraninite provide ages ranging 1.12~1.21 Ga, which is older than 0.7–0.8 Ga event well-known as major U-Pb migration in association of dolerite dyke intrusion (Bonhomme et al., 1982; Nagy et al., 1991). However, our result is consistent with previous Pb isotopic data suggesting 1.04~1.23 Ga-old event for U-Pb mobilization from three of eight galena grains of RZ10 (Gauthier-Lafaye et al., 1996).

On the other hand, the apatite has two age populations. Most parts of the apatite with non-depleted ^{235}U ($^{235}U/^{238}U=0.00725$) show an apparent mineralization age of 1.92 ± 0.01 Ga which is close to the occurrence age of reactor criticality. Another age calculated from a part of the apatite grain including excess ^{235}U ($^{235}U/^{238}U=0.00944\sim0.0182$) ranges from 0.87 to 0.98 Ga. The latter age corresponds to the chronological record of the first large migration of U and Pb around 1.1 Ga after the criticality (Nagy et al., 1991).

3.3.2. Pb minerals

It can be considered that Pb isotopic compositions in the Pb minerals have not changed since mineralization, because Pb minerals have been isolated from U after the mineralization. Therefore, the $^{207}Pb/^{206}Pb$ ratios of the Pb minerals in uraninite provide information on the occurrence age of Pb loss from uraninite. The major Pb minerals in the sample are galena (PbS). Individual galena grains, with size between 20~30 μm, were scattered throughout the uraninite matrix. Besides PbS, a rare Pb oxide mineral, minium (Pb_3O_4) occurs as a small grain along a fine fracture in apatite crystal. The presence of minium shows evidence of a highly oxidizing condition. Almost all Pb in galena and minium is radiogenic, and abundance of common Pb is very low ($^{204}Pb/^{206}Pb<0.00012$ for galena and <0.00007 for minium), which suggests that the Pb originated from uraninite. The $^{207}Pb/^{206}Pb$ ratios of galena range from 0.0850 to 0.0993, which is significantly higher than that of minium ($^{207}Pb/^{206}Pb=0.0641$ to 0.0689).

Assuming the two stage model for the galena formation from the 1.2 Ga-old uraninite with $^{235}U/^{238}U=0.0066$, the $^{207}Pb/^{206}Pb$ results show 0.45~0.83 Ga as Pb loss ages shown as T2 in Table 4. Previous Pb isotopic study reveals the age of loss of Pb studied from the distribution of Pb-Pb ages of galenas of RZ10 ranges from 0.42~1.23 Ga (Gauthier-Lafaye, 1996). Our data are in good agreement of the previous results, and suggest that the galena grains were formed in association with the intrusion of the dolerite dyke. However, it is difficult to explain formation of minium by the same event as galena.

Redox conditions of the formation of Pb minerals are restricted to low fO_2 and high fS_2 for galena, and high fO_2 and low fS_2 for minium (Garrels and Christ, 1990; Savary and

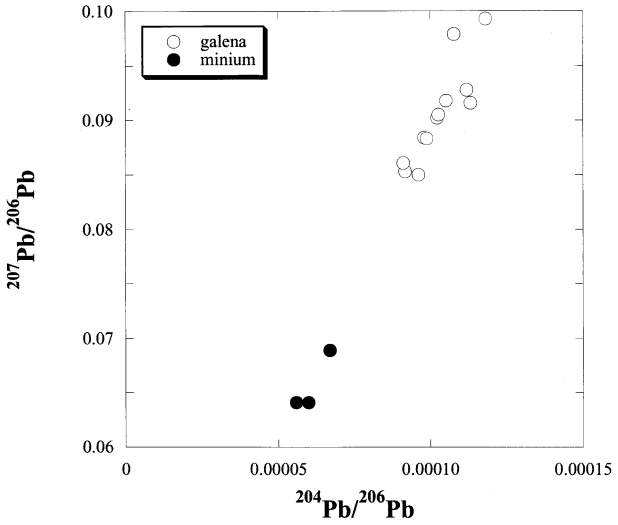

Fig. 7. $^{204}Pb/^{206}Pb$ vs. $^{207}Pb/^{206}Pb$ diagram of galena and minium.

Pagel, 1997). Because the formation condition for minium is quite different from that of galena, it is impossible to consider the simultaneous mineralization of galena and minium. If the minium was formed by released radiogenic Pb from the 1.2 Ga-old uraninite, the low $^{207}Pb/^{206}Pb$ ratios (0.0641∼0.0689) of minium cannot be explained. It may be conceivable that minium was formed later than galena. The comparison of the Pb isotopic data between galena and minium may provide key information of the origin of minium. Figure 7 shows $^{204}Pb/^{206}Pb$ vs. $^{207}Pb/^{206}Pb$ diagram of galena and minium measured in this study. The data sets of galena and minium grains seem to be plotted on the same single line, although the data of minium are limited. The precipitation of minium is due to very oxidizing environment that probably occurs only close to the uraninites where the radiolytic effect is efficient. This is reasonable, because it is known that oxygen formed by radiolysis of water in the vicinity of the RZ (Dubessy et al., 1988; Savary and Pagel, 1997; Pourcelot and Gauthier-Lafaye, 1998). The oxygen due to radiolysis of water was stored and played a role in changing the oxidizing conditions. The oxidizing environment to form minium is considered to be very local because of the rare existence of minium. Unfortunately we cannot make more conclusive discussion for the origin of minium, because the number of data for minium in the sample is limited.

4. CONCLUSIONS

Isotopic analyses of REE, U and Pb in uraninite, apatite and Pb minerals provide geochemical information on the migration behavior of radionuclides and chronological data of U-Pb mobilization in association with the intrusion of dolerite dyke. Sm and Gd isotopic ratios of uraninite and apatite show strong evidence of neutron irradiation with fluence of $4.4-6.8\times10^{19}$ n/cm^2. Pb isotopic data of uraninite, apatite and Pb minerals do not directly reflect the individual formation ages, but their systematic interpretation puts constraints on the alteration history around the boundary between uraninite and sandstone.

The Pb isotopic signature suggests that the apatite concretion at the boundary is 1.92 Ga-old and has survived in spite of dissolution of uraninite. From REE and U isotopic analysis, it can be concluded that fissiogenic LREE and nucleogenic Pu were selectively trapped into the apatite grain during the criticality of reactor.

Isotopic homogeneity of $^{235}U/^{238}U$, concentrated U matrix, and significant variation of $^{207}Pb/^{206}Pb$ ratios in the uraninite suggest that the uraninite dissolved at least once around the boundary layer between RZ and sandstone, and chemical fractionation occurred between U and Pb in the uraninite. $^{207}Pb/^{206}Pb$ ratios for the uraninite show an apparent age of 1.12∼1.21 Ga. Galena grains in the uraninite were formed by U-Pb mobilization in association with the dolerite dyke intrusion 0.45∼0.83 Ga ago.

Table 4. Pb isotopic ratios of minimum and galena and age of Pb loss from uraninite.

	$^{204}Pb/^{206}Pb$	$^{207}Pb/^{206}Pb$	$^{208}Pb/^{206}Pb$	Age T2 (Ma)
minimum				
01	0.0000665 ± 15	0.0689 ± 3	0.00332 ± 3	
02	0.0000560 ± 9	0.0641 ± 2	0.00297 ± 2	
03	0.0000596 ± 15	0.0641 ± 2	0.00298 ± 3	
galena				
01	0.0001052 ± 8	0.0918 ± 2	0.00531 ± 2	664 ± 5
02	0.0000980 ± 11	0.0884 ± 3	0.00513 ± 2	561 ± 9
03	0.0001132 ± 9	0.0916 ± 3	0.00538 ± 2	658 ± 8
04	0.0001120 ± 15	0.0928 ± 2	0.00544 ± 1	693 ± 5
05	0.0001023 ± 15	0.0902 ± 2	0.00520 ± 2	616 ± 6
06	0.0000918 ± 9	0.0853 ± 2	0.00467 ± 3	462 ± 6
07	0.0000989 ± 7	0.0883 ± 4	0.00501 ± 5	558 ± 12
08	0.0001182 ± 10	0.0993 ± 2	0.00600 ± 2	870 ± 5
09	0.0000912 ± 20	0.0861 ± 1	0.00479 ± 3	488 ± 3
10	0.0000961 ± 10	0.0850 ± 2	0.00475 ± 2	453 ± 6
11	0.0001027 ± 10	0.0905 ± 2	0.00521 ± 3	625 ± 6
12	0.0001078 ± 21	0.0979 ± 2	0.00583 ± 2	833 ± 5

T2 is age of Pb loss for uraninite presumably dissolved at 1.2 Ga (T1) with $^{235}U/^{238}U = 0.0066$. T2 was calculated by the following equation: $^{207}Pb/^{206}Pb = 0.0066 \times (\exp(\lambda_5 T_1) - \exp(\lambda_5 T_2))/(\exp(\lambda_8 T_1) - \exp(\lambda_8 T_2))$ where λ_5 and λ_8 are decay constants of ^{235}U and ^{238}U, respectively.
All standard errors indicated the last digit are 1σ of the mean.

A changing of redox conditions possibly due to radiolysis of water can be concluded from the co-existence of minium and galenas in the sample. The Pb isotopic compositions of Pb minerals suggest that the minium was derived from galena under locally oxidizing conditions.

Acknowledgments—We are grateful to R. Bros (JNC, Tokai) for preparation of the thin section sample. Thanks are expressed to Y. Shibata and J. Ando for their technical helps with EPMA and micro-Raman analyses. Critical reading and constructive comments by J. Janeczek, M. Pagel, and two anonymous journal reviewers were very helpful to improve the first draft of this paper. The suggestions from the Associate Editor, B. Marty were useful in revising the manuscript. A part of this study was financially supported by a Grant-in-Aid for Ministry of Education, Culture, Sports, Science and Technology (to H.H., No. 13440167).

Associate editor: B. Marty

REFERENCES

Bodu R., Bouzigues H., Morin N. and Pfiffelmann J. P. (1972) Sur l'existence d'anomalies isotopiques rencontrées dans l'uranium du Gabon. *C. R. Acad. Sci. Paris* **275,** Série D,1731–1734.

Bonhomme M., Gauthier-Lafaye F., and Weber F. (1982) An example of Lower Proterozoic sediments: the Francevillian in Gabon. *Precamb. Res.* **18,** 87–102.

Bros R., Gauthier-Lafaye F., Holliger P., and Still P. (1993) Occurrence of naturally enriched ^{235}U: Implications for plutonium behavior in natural environments. *Geochim. Cosmochim. Acta* **57,** 1351–1356.

Bros R., Carpena J., Sere V., and Beltritti A. (1996) Occurrence of Pu and fissiogenic rare earth elements in hydrothermal apatites from the fossil natural nuclear reactor 16 of Oklo (Gabon). *Radiochim. Acta* **74,** 277–282.

Chapman N. A. and Smellie J. A. T. (1986) Introduction and summary of the workshop, Natural analogues to the conditions around a final repository for high-level radioactive waste. *Chem. Geol.* **55,** 167–173.

Cramer J. J. and Smellie J. A. T. (1992) The AECL/SKB Cigar Lake analogue study. Some implications for performance assessment, EUR proceedings of the 5th CEC Natural Analogue Working Group, Toledo, Spain. Oct. 6–9.

Curtis D. B., Benjamin T. M., Gancarz A. L., Loss R. D., Rosman K. J. R., DeLaeter J. R., Delmore J. E., and Maeck W. J. (1989) Fission product retention in the Oklo natural reactors. *App. Geochem.* **4,** 49–62.

Dubessy J., Pagel M., Beny J. M., Christensen H., Hickel B., Kostolanyi C., and Poty B. (1988) Radiolysis evidenced by H_2-O_2 and H_2-bearing fluid inclusions in three uranium deposits. *Geochim. Cosmochim. Acta* **52,** 1155–1167.

Dymkov Yu., Holliger P., Pagel M., Gorshkov A., and Artyukhina A. (1997) Characterisation of a La-Ce-Sr-aluminous hydroxy phosphate in nuclear zone 13 in the Oklo uranium deposit (Gabon). *Min. Depos.* **32,** 617–620.

England T. R. and Rider B. F. (1993) Evaluation and compilation of fission product yields. ENDF-349, LA-UR-94–3106.

Felitsyn S. and Morad S. (2002) REE patterns in latest Neoproterozoic-early Cambrian phosphate concretions and associated organic matter. *Chem. Geol.* **187,** 257–265.

Garrels R. M. and Christ C. (1990) Solutions, Minerals, and Equilibria (2nd edition). Jones & Bartlett Pub., pp. 464.

Gauthier-Lafaye F., Holliger P., and Blanc P. L. (1996) Natural fission reactors in the Franceville basin, Gabon: A review of the conditions and results of a "critical event" in a geological system. *Geochim. Cosmochim. Acta* **60,** 4831–4852.

Hidaka H., Masuda A., Fujii I., and Shimizu H. (1988) Abundance of fissiogenic and pre-reactor natural rare-earth elements in auranium ore sample from Oklo. *Geochem. J.* **22,** 47–54.

Hidaka H., Holliger P., Shimizu H., and Masuda A. (1992) Lanthanide tetrad effect observed in the Oklo and ordinary uraninites and its implication for their forming processes. *Geochem. J.* **26,** 337–346.

Hidaka H., Holliger P., and Masuda A. (1993) Evidence of fissiogenic Cs estimated from isotopic deviations in a Oklo natural Reactor zone. *Earth Planet. Sci. Lett.* **114,** 391–396.

Hidaka H., Takahashi K., and Holliger P. (1994) Migration of fission products into micro-minerals of the Oklo natural reactors. *Radiochim. Acta* **66/67,** 463–468.

Hidaka H., Ebihara M., and Shima M. (1995) Determination of isotopic compositions of Sm and Gd by thermal ionization mass spectrometry. *Anal. Chem.* **67,** 1437–1441.

Hidaka H. and Holliger P. (1998) Geochemical and neutronic characteristics of the natural fossil fission reactors at Oklo and Bangombé, Gabon. *Geochim. Cosmochim. Acta* **62,** 89–108.

Hidaka H., Holliger P., and Gauthier-Lafaye F. (1999) Tc/Ru fractionation in the Oklo and Bangombé natural fission reactor, Gabon. *Chem. Geol.* **155,** 323–333.

Hidaka H. and Gauthier-Lafaye F. (2000) Redistribution of fissiogenic and non-fissiogenic REE, Th and U in and around natural fission reactors at Oklo and Bangombé, Gabon. *Geochim. Cosmochim. Acta* **64,** 2093–2108.

Holliger P. and DeVillers C. (1981) Contribution à l'étude de la température dans les réactuers fossiles d'Oklo par la mesure du rapport isotopique du lutetium. *Earth Plan. Sci. Lett.* **52,** 76–84.

I.A.E.A.(International Atomic Energy Agency) (1975) SM-204:Le Phénomènon d'Oklo. Proc. Tech. Comm. STI/PUB/405.

I.A.E.A.(International Atomic Energy Agency) (1978) TC-119:Natural Fission Reactors. Proc. Tech. Comm. STI/PUB/475.

Janeczek J. (1999) Natural Fission Reactors in Gabon. In *Uranium: Mineralogy, Geochemistry and the Environment* (eds. P. C. Burns and R. Finch) Reviews in Mineralogy Vol. 38, P.321–392.

Janeczek J. and Ewing R. C. (1996) Florencite-(La) with fissiogenic REEs from a natural fission reactor at Bangombé, Gabon. *Am. Mineral.* **81,** 1263–1269.

Leng A. H., Griffith J. W. and Steacy H. R. (1962) Faraday Mine. In *Canadian Deposits of Uranium and Thorium* (ed. R. Duhamel) Economic Geology Series No. 16. P. 182–184.

Loss R. D., Rosman K. J. R., DeLaeter J. R., Curtis D. B., Benjamin T. M., Gancarz A. L., Maeck W. J., and Delmore J. E. (1989) Fission product retentivity in peripheral rocks at the Oklo natural fission reactors, Gabon. *Chem. Geol.* **76,** 71–84.

Loubet M. and Allegre C. (1977) Behavior of the rare earth elements in the Oklo natural reactor. *Geochim. Cosmochim. Acta* **41,** 1539–1548.

Lugmair G. W. and Marti K. (1977) Sm-Nd-Pu timepieces in the Angra dos Reis meteorite. *Earth Planet. Sci. Lett.* **35,** 273–284.

Maravic H. Von and Smellie J. A. T. (1992) Alligator River Analogue Project Final Workshop, EUR proceedings of the 5th CEC Natural Analogue Working Group, Toledo, Spain. Oct. 5–8.

Masuda A. and Ikeuchi Y. (1979) Lanthanide tetrad effect observed in maarine environment. *Geochem. J.* **13,** 19–22.

McArthur J. M. and Walsh J. N. (1984) Rare-earth geochemistry of phosphorites. *Chem. Geol.* **47,** 191–220.

Menet C., Menager M.-T., and Petit J.-C. (1992) Migration of radioelements around the new nuclear reactors at Oklo: Analogies with a high-level waste repository. *Radiochim. Acta* **58/59,** 395–400.

Nagy B., Gauthier-Lafaye F., Holliger P., Davis D. W., Mosmann D. J., Leventhal J. S., Rigali M. J., and Parnell J. (1991) Organic matter and containment of uranium and fissiogenic isotopes at the Oklo natural reactors. *Nature* **354,** 472–475.

Naudet R. (1991) Oklo: des réacteurs nucléaires fossiles. Collection du Commissariat à l'Energie Atomique Paris.

Neuilly M., Bussac J., Fréjacques C., Nief G., Vendryes G. and Yvon J. (1972) Sur l'existence dans un passé reculé d'une réaction en chaine naturelle de fissions dans le gisement d'uranium d'Oklo (Gabon). *C. R. Acad. Sci. Paris* **275,** Série D 1847–1849.

Pourcelot L. and Gauthier-Lafaye L. (1998) Mineralogical, chemical and O-isotopic data on uraninites from Natural Fission Reactors (Gabon): Effects of weathering conditions. *C. R. Acad. Sci. Paris* **326,** Série D,485–492.

Raimbault L., Peycelon H., and Blanc P. L. (1996) Characterization of near- to far-field ancient migrations around Oklo reaction zones (Gabon) using minerals as geochemical tracers. *Radiochim. Acta* **74,** 283–287.

Sano Y., Oyama T., Terada K., and Hidaka H. (1999) Ion microprobe U- Pb dating of apatite. *Chem. Geol.* **153,** 249–258.

Savary V. and Pagel M. (1997) The effects of water radiolysis on local redox conditions in the Oklo, Gabon, natural fission reactors 10 and 16. *Geochim. Cosmochim. Acta* **61,** 4479–4494.